This is an author produced version of a paper published in Journal of Hydrology. This paper is the final submitted version before typesetting and journal pagination. The published paper can be found at: https://doi.org/10.1016/j.jhydrol.2018.07.071

Full citation for the published paper :

Mas, A., Baraer, M., Arsenault, R., Poulin, A. and Prefontaine, J., 2018. Targeting high robustness in snowpack modeling for Nordic hydrological applications in limited data conditions. *Journal of Hydrology*, *564*, pp.1008-1021.

Targeting high robustness in snowpack modeling for Nordic hydrological applications in limited data conditions

Alexandre Mas[a], Michel Baraer[a*], Richard Arsenault[a], Annie Poulin[a] and Jonathan Préfontaine[a]

[a] Department of Construction Engineering, École de technologie supérieure, University of Quebec, 1100 Notre-Dame Street West, Montreal, QC, H3C 1K3, Canada.

[*] Corresponding author; email address: Michel.baraer@etsmtl.ca

Abstract

Most hydrological models simulate snowmelt using a degree day or simplified energy balance method, which usually requires a calibration of snow-related parameters using discharge data. Despite its apparent efficiency, this method leads to empirical relations which are not proven to remain valid in a changing climate. The direct application of robust physically-based snow models in hydrological modeling is difficult due to the high number of not easily available input variables this model type requires. The objective of this study is to test the robustness of a physically-based snowpack model that requires only a limited number of common meteorological parameters. The MASiN model computes the energy and mass balance of multiple layers of the snowpack using hourly air temperature, relative humidity and wind speeds, as well as daily precipitations. MASiN was tested at 23 sites across Canada and Sweden, using a unique set of parameters fixed at a single site. At each site, the snow depth simulated by MASiN was compared against measurements. Robustness was challenged by comparing MASiN's performance to that of three other models on three different criteria. MASiN showed the highest robustness among the tested models. With a unique set of parameters, it showed better results than the three reference models when used in similar conditions and matched their performances when reference models were calibrated at each site. The results prove non-data intensive physically based models to be promising tools for hydrological and other snow cover-related studies.

1. Introduction

In Nordic regions, most precipitation occurs as snow during winter. Snow accumulation for these regions represents a major portion of the watershed water storage (Ferguson, 1999) . The release of melt water at the end of the winter period drives the hydrology of snow-covered catchments as well as downstream areas with little or no snow (Thompson et al., 2000). In snow-dominated regions, both surface runoff and groundwater flow are strongly influenced by the amount of melt water released and its temporal distribution (Dingman, 2002; Lundberg et al., 2016). In a context where Nordic regions exhibit deep vulnerability to climate change (Minder, 2010; Stone et al., 2002), it is necessary to properly simulate the evolution of snow cover in hydrological models, to be able to anticipate changes in water resources, flood risks and ecosystems (Ferguson, 1999; Shamir and Georgakakos, 2006; Troin et al., 2016).

The phenomena occurring inside a snowpack, the interaction between a snowpack and its environment, as well as general snow physics, have been extensively studied in order to address specific snow hydrology problems (DeWalle and Rango, 2008). The current state of the art is that we can adequately, often even expertly, model snowmelt when we have the requisite input data (Sturm, 2015).

Traditionally, models simulating the evolution of a snowpack can be classified into two categories: conceptual models (CO) and energy balance (EB) models, also called physically-based models (Ohara and Kavvas, 2006). EB models developed over the last decades have proven to be highly accurate in snowpack characteristics modeling (Langlois et al., 2009). Different physically-based models, such as the "point energy and mass balance model of a snow cover" (Anderson, 1976), CROCUS (Brun et al., 1989), SNOWPACK (Bartelt and Lehning, 2002) or SNTHERM (Jordan, 1991), among others, have been developed to simulate the evolution of a snow cover for demanding applications such as avalanche prediction.

Despite their recognized performances, full EB approaches are demanding in terms of data collection and computations. For many applications in hydrology, detailed methods are simply not feasible, and simpler methods are required (Bavera et al., 2014; Franz et al., 2008; Meeks et al., 2017; Morin, 2014; Raleigh et al., 2016; Tobin et al., 2013).

CO models rely mainly on empirical relationships to estimate the amount of accumulated and melted snow at a given time step (Hock, 2003). They require a calibration of their parameters against measurements in order to provide good simulated values. They can be subdivided into empirical (EM), temperature index (TI) and enhanced TI (ETI) models. EM models simply compute a unique snow characteristic like the depth of the snowpack (SD) or the snow water equivalent (SWE) based on a single equation, not specifically conveying any physical meaning (e.g. Baraer et al., 2010; Scott et al., 2003). TI models are based on simple or enhanced degree day methods, as in CEMANEIGE (Valéry, 2010), HBV (Bergström, 1976) and SRM (Martinec and Rango, 1986). TI models associate linear relationships between ablation and air temperature, usually expressed in the form of positive temperature sums (Hock, 2003). ETI models are often adaptations of the traditional TI models that aim to overcome the model's simplicity and consequent limitations (Meeks et al., 2017). Model enhancements are achieved by incorporating additional input variables into melt equations (Brubaker et al., 1996; Machguth et al., 2006; Pellicciotti et al., 2005; Singh et al., 2009) and/or adding temperature-based equations for simulating processes involved in snowpack conditions (Hock, 2003; Hood and Hayashi, 2015; Mosier et al., 2016; Rutter et al., 2009; Tobin et al., 2013; Turcotte et al., 2007). The use of CO models presents two principal advantages. They usually require simple meteorological data, such as the daily precipitation and the air temperature (daily mean or daily maximum). Using CO models also makes for short and simple formulations, meaning that the model is usually not demanding in terms of computation time (Hock, 2003). Different studies have shown that, despite their simplicity, CO models are efficient in simulating SWE evolution in time (Debele et al., 2010; Troin et al., 2016; Watson and Putz, 2014; Williams and Tarboton, 1999). Despite the obvious advantages CO models propose, concerns have been expressed relating to the fact that quantities known to influence the energy balance and snowmelt processes, such as vapor pressure, wind and reflected radiation, are neglected (Tobin et al., 2013). Moreover, recourse to extensive calibration often makes CO models less robust and raises the question of their transferability in space and time (Mauser and Bach, 2009), and their ability to provide good predictions in a changing climate has been questioned (Bougamont et al., 2007;

Ludwig et al., 2009). Snow accumulation, duration of snow cover period and snowmelt processes are expected to be strongly affected by the projected global warming trend during the 21st century (Adam et al., 2009; Barnett et al., 2005; Pohl et al., 2006). Empirical relationships that are currently used in CO models are derived from calibration using past and present conditions, and may no longer be valid in the context of future climate conditions (Warscher et al., 2013). In hydrological models, key parameters, including those describing snow, are generally calibrated against discharge measurements (Saelthun et al., 1998), and calibration of snow parameters solely at the basin outlet does not necessarily lead to optimal performances (Franz and Karsten, 2013). The snow parameters are thus sensitive to equifinalities, and can lead to unreasonable snow cover evolution estimations (Finger et al., 2015; Konz et al., 2010). Even the use of ETI models in such conditions does not necessarily improve the overall performance of hydrological models. In general, including too many parameters requiring calibration against stream discharge causes an increase in the number of undefined parameters, which can lead to over-fitting and poor predictive capabilities of the hydrological models (Magnusson et al., 2014).

Recently, increasing attention has been paid to multi snowpack models and ensemble modeling approaches in the literature (Essery et al., 2013; Franz et al., 2010; Magnusson et al., 2014). These methods allow the inter-comparison of different model types and an estimation of the modeling uncertainties associated with the various sources of error in the forecasting process (Franz et al., 2010). However, the direct applicability of such ensemble modeling approaches to hydrology appears uncertain as they increase the computational demand while still requiring difficult-to-access meteorological parameters.

To date, the datasets required to run multiple concurrent model types have limited such approaches to a restricted number of sites and to limited periods (Essery et al., 2016). Also, useful insights have been gained; snowpack model comparisons have generally failed to find clear relationships between model complexity and performance and have not succeeded in finding an overall best model (Essery, 2015).

Despite all efforts and recent advances in snowpack modeling, the choice for hydrological modelers remains mainly between CO models of different complexities and data intensive EB models. Moving ahead from this dilemma requires integrating a more process-based approach into the development of snowpack models for hydrology (Mendoza et al., 2014; Sturm, 2015). After testing 1701 different model combinations, Essery et al. (2013) concluded that models including prognostic equations for changes in snow density and albedo, and that take some account of storage and refreezing of liquid water, perform better than simpler models. Meeks et al. (2017) claim that snowmelt modeling uncertainty may be reduced by the inclusion of more data that allow the use of more complex approaches such as the energy balance method. Lundberg et al. (2016) conclude a literature review on snow and frost by underlining that process-based models are more suited than CO models for different applications such as modeling rain-on-snow events or heat advection from bare soils.

Introducing empirical relationships into EB models to compensate for the lack of input data availability offers the possibility of moving toward more process-based modeling in snowpack hydrology (Förster et al., 2014; Raleigh et al., 2016). While not designed for feeding common hydrological models, snowpack models proposed by Jacobi et al. (2010)

and Strasser and Marke (2010) have demonstrated that this approach might represent an interesting solution.

Another method for developing more process-based snowpack models involves keeping EB snowpack models as simple as possible by designing them based on their intended application (Magnusson et al., 2014). EB models dedicated to avalanche forecasting, for example, describe snow grain size and type, characteristics that have not been reported as critical for hydrological applications (e.g. Essery et al., 2013).

In the present study, we target non-mountainous Nordic hydrological applications in designing a process-based snowpack model named MASiN (Modèle Autonome de Simulation de la Neige). The objective is to move toward the high robustness associated with pure EB models (Hood and Hayashi, 2015) with a model applicable to sites where only simple metrological variables are available. Using a survey presented by Raleigh et al. (2016) on Automatic Weather Stations across over the western United States, we selected the air temperature, precipitation, wind speed and relative humidity as model input variables. According to the survey, 35% of the 1318 studied stations that measure SWE also provide those variables, whereas only 24% also measure incoming solar radiation.

Targeting hydrological applications limits the requirement for output variables to SWE, snow depth and melt water outflow volumes. Finally, targeting non-mountainous environments allows keeping coverage processes reasonable by, for example, not accounting for slope effects. Because model robustness cannot be tested on the very limited number of sites where long SWE time series exist, the model performance was assessed by evaluating its ability to estimate the more commonly measured snow depth, the close second most fundamental metric used to characterize the hydrological role of snow (Sturm et al., 2010).

Ultimately, the MASiN model's robustness was assessed by setting a unique set of parameters on a single site and comparing its performance to other models (1) calibrated following the same protocol and (2) specifically calibrated on each test site.

2. Model presentation

2.1 Overview

MASiN uses the hourly air temperature, relative humidity, wind speed and daily precipitations to simulate the evolution of a snowpack at a given point using the energy and mass balance method. The following outputs are provided on an hourly time basis: SD, SWE, water outflow, evaporation, temperature and density profiles of the snowpack. The snowpack is modeled using a multi-layer approach, with layers being dynamically managed to respect a maximum number of layers and a minimum depth. Based on a sensitivity analysis, the model parameters are either set to values from the literature or adjusted at one of the study sites and then left unchanged.

The following are some notations to which we will refer throughout this paper:

- Δt is the sub-time step
- n is the total number of layers
- The subscripts t and $t+1$ are used to refer to values at the beginning and at the end of a computational time step, respectively

- Layers are numbered from 1 to n from the base of the pack to the top, with superscript *i* being used to refer to the layer considered
- *T* is the layer temperature
- *M* is the amount of melted snow of the layer
- *SWE* is the snow water equivalent of the layer
- *LW* is the liquid water content of the layer
- *LWHC* is the liquid water holding capacity of the layer

2.2 Computation frame

The main computation steps of the model are presented in Fig. 1.

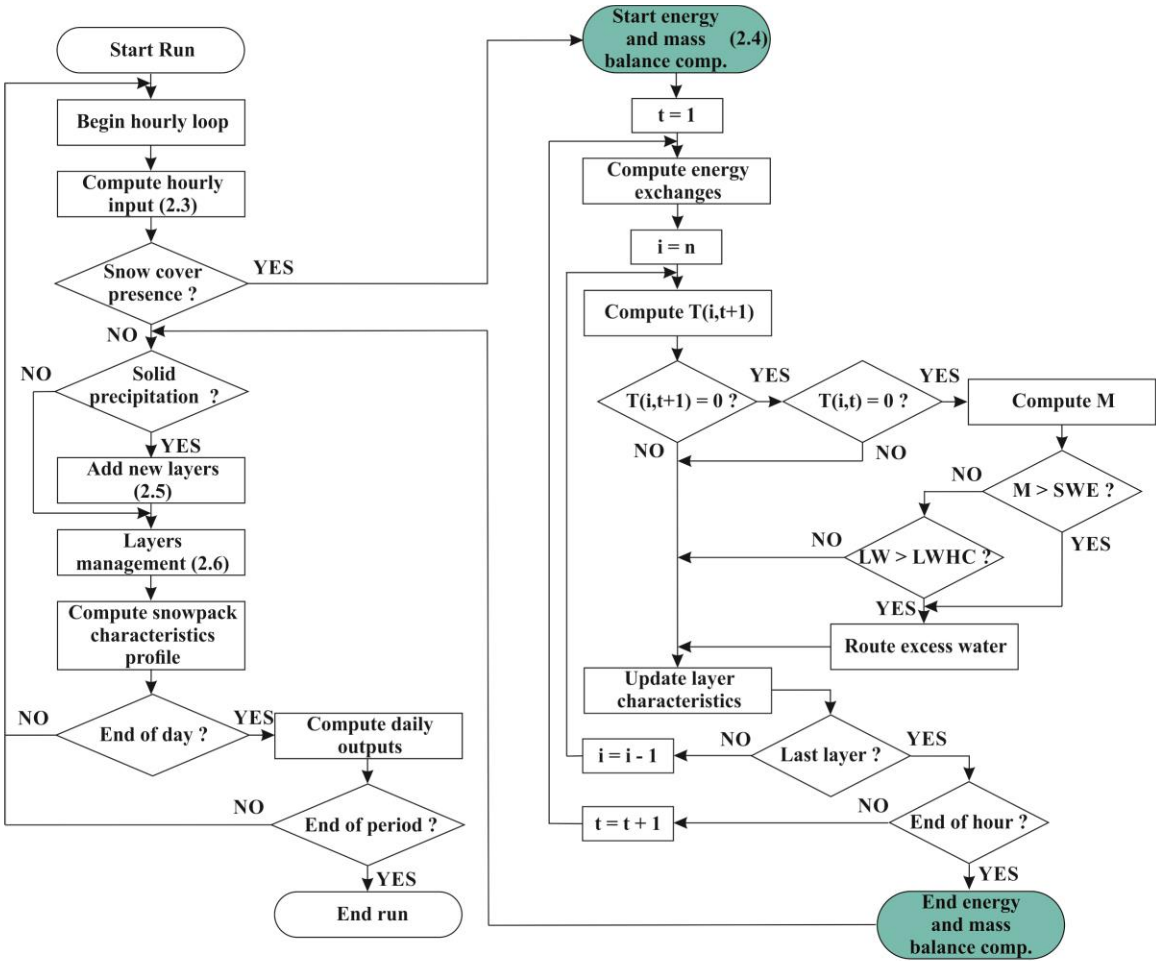

Fig. 1. Simplified flowchart of MASiN running procedure. The blue boxes correspond to the start and the end of the energy and mass balance computation.

At the beginning of each hour of the simulation period, the precipitation intensity and incoming shortwave radiations are computed following the procedure detailed in section 2.3. If a snowpack is present, the energy and mass balance of each layer is then computed (section in-between blue boxes in Fig. 1.) using an iterative explicit forward scheme which provides a simple formulation and ease of modification. The drawback is that due to the non-linearity of energy transfers, a very short computational time step of 30 seconds is necessary to ensure a good accuracy. Details concerning the calculations of the energy and mass balance of the layers are provided in section 2.4. At the end of each hour, prospective solid precipitation is added to the snowpack, as presented in section 2.5. The layers are then managed as explained in detail in section 2.6. Finally, hourly snow characteristics and profiles are computed by taking the mid-hour values of the parameters. Section 2.7 presents the parameterization process of the model.

2.3 Input dataset

Hourly air temperature, wind speed and relative humidity are taken directly from weather stations measurements. As hourly precipitations are seldom available, these are computed from daily measurements, as shown in section 2.3.1. The computation of incoming shortwave radiations is detailed in section 2.3.2.

2.3.1 Hourly precipitation computation

MASiN can use both total and separated precipitation. If separated daily precipitations are available, total rain is equally distributed over 24 hours, and total snow is distributed over as many hours as possible, provided the minimal layer height is respected. Otherwise, total snow depth is divided into as many hourly precipitations as possible, while respecting the minimal height rule, as is described later in this paper.

If only the total daily precipitation is available, it is equally distributed over the 24 hours of the day. When the hourly temperature is below 1°C, precipitation is in the form of snow, otherwise, it occurs as rain. If needed, a redistribution of snow is done over the hours for which the air temperature is below 1°C, ensuring the creation of new layers.

2.3.2 Shortwave radiations computation

In the MASiN model, shortwave radiations are computed according to the potential solar radiation theory proposed by Lee (1963). As atmospheric effects are not considered by the chosen formulation, parameters have been added to take into account the effect of cloud cover. A separation between direct and diffuse radiations is carried out, as some of the snow properties (e.g., albedo and absorption of solar radiation) change with the radiation type (Sergent et al., 1987).

2.3.2.1 Extra-terrestrial irradiation

The extra-terrestrial shortwave radiation $I_{sw,cs}$ in W m^{-2} is computed as:

$$I_{sw,cs} = \frac{I_0}{e^2} \cos Z \tag{1}$$

where I_0 is the solar constant (W m^{-2}), e is an adjustment parameter assessing the effect of the sun-earth distance variation throughout the year, and Z is the zenith angle. The latter is expressed as a combination of three other angles, as shown in equation 2.

$$\cos Z = \sin\theta \sin\delta + \cos\theta \cos\delta \cos\omega t \tag{2}$$

where θ is the latitude, δ is the sun declination and ωt is the hour angle. The latter two depend mainly on the hour of the day and the day of the year.

2.3.2.2 Effect of cloud cover and vegetation

The extra-terrestrial radiation is adjusted as a function of nebulosity and vegetation to compute the incoming shortwave radiation I_{sw} (W m^{-2}):

$$I_{sw} = k_{sw} I_{sw,cs} (\mathrm{e}^{-k_{veg} LAI}) \tag{3}$$

where k_{sw} is the cloud cover factor and k_{veg} and LAI represent the effect of vegetation. Nebulosity is assessed using the cloud cover *Cc*, which represents the fraction of the sky that is covered by clouds, with a value of 0 representing completely clear sky and a value of 1 representing overcast sky. Its value and its corresponding coefficient k_{sw} are determined using the daily air temperature range ΔT. The method is derived from that proposed by Bristow and Campbell (1984). When ΔT is below the threshold ΔT_{Ccmax}, the cloud cover equals 1 and k_{sw} is set to its minimal value $k_{sw\,min}$. When ΔT is above the threshold ΔT_{Ccmin}, the cloud cover equals 0 and k_{sw} is set to its maximal value $k_{sw\,max}$. Between the thresholds, the evolution of *Cc* and k_{sw} is linear. As the sensitivity of the model output to the thresholds value is rather high, these two parameters are computed for each winter as follows:

$$\Delta T_{Ccmin} = \frac{\sum_{\mathrm{i}=1}^{\mathrm{N}_1} \Delta T_i}{\mathrm{N}_1} \tag{4}$$

where ΔT is the daily air temperature range of the N_1 winter days for which the total precipitation is more than 2 mm.

$$\Delta T_{Ccmax} = \frac{\sum_{\mathrm{i}=1}^{\mathrm{N}_2} \Delta T_i}{\mathrm{N}_2} \tag{5}$$

where N_2 is the 10% of winter days with the highest daily air temperature range ΔT.

Maximal and minimal k_{SW} values are adjusted at model parameterization. The separation between direct and diffuse radiation $I_{sw,dir}$ and $I_{sw,dif}$ is performed as follows:

$$\begin{aligned} I_{sw,dir} &= k_{dir} I_{sw} \\ I_{sw,dif} &= (1 - k_{dir}) I_{sw} \end{aligned} \tag{6}$$

This expression is derived from the polynomial equation proposed by Linacre (1992), which is very close to linearity in the range of values we consider. The coefficient k_{dir} varies linearly between a minimum value $k_{dir,min}$ when the cloud cover equals 1, and a maximum value $k_{dir,max}$ when the cloud cover equals 0. $k_{dir,min}$ and $k_{dir,max}$ are set during the parameterization phase.

2.3.2.3 Net shortwave radiation

Part of the incoming shortwave radiation I_{sw} is reflected as a function of the snow albedo. The shortwave radiation that penetrates the pack Q_{nsi} is the sum of the direct and diffuse radiation $Q_{nsi,dir}$ and $Q_{nsi,dif}$:

$$\begin{aligned} Q_{nsi,dir} &= I_{sw,dir}(1 - a_{dir}) \\ Q_{nsi,dif} &= I_{sw,dif}\left(1 - a_{dif}\right) \end{aligned} \tag{7}$$

where a_{dir} and a_{dif} are the albedos for direct and diffuse radiations. They are both computed using a relation adapted from U.S. Army Corps of Engineers (1956), shown in equation 8:

$$a_{dir} = a_{min,dir}\left(1 + \mathrm{e}^{-0.1\frac{A}{24}}\right)$$
$$a_{dif} = a_{min,dif}\left(1 + \mathrm{e}^{-0.1\frac{A}{24}}\right) \quad (8)$$

where $a_{min,dir}$ and $a_{min,dif}$ are the minimum albedos for direct and diffuse radiations, and A is the age of the top layer of the snowpack. A is expressed as the number of hours since the layer was added to the pack. The minimum albedos $a_{min,dir}$ and $a_{min,dif}$ are set during the parameterization phase.

2.4 Energy and mass balance computation

The energy and mass balance function of MASiN runs as presented in Fig. 1. This calculation loop is performed at a computational time step Δt for each hour of the simulation step.

The energy exchanges between the layer i and its surroundings are first computed in order to assess the layer internal energy variation Q^i, as shown in equation 9 (Brun et al., 1989)

$$\begin{aligned} Q^i &= Q_{ns} + Q_{nl} + Q_h + Q_e + Q_w + Q_c && \text{for the top layer} \\ Q^i &= Q_{ns} + Q_w + Q_c + Q_g && \text{for the bottom layer} \\ Q^i &= Q_{ns} + Q_w + Q_c && \text{for the intermediate layer} \end{aligned} \quad (9)$$

where all terms are in W m^{-2}. Q_{ns} is the net shortwave flux, Q_{nl} is the net longwave flux, Q_h and $Q_e$are the sensible and latent heat fluxes, $Q_w$is the energy flux due to liquid water inputs, and Q_c and Q_g are the conduction heat fluxes between the layers and between the snowpack and the ground.

It is then possible to compute the temperature variation ΔT^i and the liquid water content variation ΔLW^i in the layer following equation 10 (Barry et al., 1990).

$$Q^i = c_t^i \rho_t^i H_t^i \frac{\Delta T^i}{\Delta t} + l_f \rho_w \frac{\Delta LW^i}{\Delta t} \tag{10}$$

where c_t^i is the snow-specific heat (J kg^{-1} K^{-1}), ρ_t^i is the snow density (kg m^{-3}), H_t^i is the layer thickness (m), l_f is the latent heat of fusion of water (J kg^{-1}) and ρ_w is the water density (kg m^{-3}). As ΔT^i and ΔLW^i are both unknown in equation 10, it is not possible to solve for both T_{t+1}^i and LW_{t+1}^i. The computational time step thus needs to be short enough to consider that temperature and phase changes do not occur simultaneously. Using a time step of thirty seconds was shown to render the error due to this computational choice acceptable. The computational choices in terms of the energy exchange terms of the right-hand side of equation 9 are provided in section 2.4.1. Once the internal energy variation of the layer is computed, its mass balance is computed, depending on whether or not melt occurs, as explained in section 2.4.2. The settling of the layer is taken into account, as presented in section 2.4.3.

2.4.1 Energy exchanges terms

2.4.1.1 Shortwave radiations

The fraction of incident radiation which is absorbed by a snow layer corresponds to the difference between the transmittances at its upper and lower depths (Dunkle and Bevans, 1956). The total shortwave radiation absorbed by a layer of thickness H_t^i at a mean depth of z_t^i can therefore be expressed as follows (Giddings and LaChapelle, 1961) :

$$\begin{aligned} Q_{ns} &= Q_{nsi,dir}\left[\mathrm{e}^{-\beta_{dir}\,(z_t^i-H_t^i/2)} - e^{-\beta_{dir}\,(z_t^i+H_t^i/2)}\right] \\ &+ Q_{nsi,dif}\left[\mathrm{e}^{-\beta_{dif}\,(z_t^i-H_t^i/2)} - e^{-\beta_{dif}\,(z_t^i+H_t^i/2)}\right] \end{aligned} \tag{11}$$

where β_{dir} and β_{dif} are the absorption coefficients for direct and diffuse radiations, respectively. They are set during the model parameterization.

2.4.1.2 Longwave radiations

Longwave radiations are computed using Stefan-Boltzmann law. The snowpack is assumed to be a black body with an emissivity $\epsilon = 1$. The net longwave radiative flux is:

$$Q_{nl} = \epsilon_a \sigma {T_a}^4 - \sigma {T_t^n}^4 \tag{12}$$

where ϵ_a is the atmospheric emissivity, T_a and T_t^n are the air and snow surface temperatures (K), and σ is the Stefan-Boltzmann constant. The atmospheric emissivity is computed with the formula of Brutsaert (1975) modified to account for the cloud cover Cc (Liston and Elder, 2006; Oke, 2002):

$$\epsilon_a = 1.72\left(\frac{e_a}{T_a}\right)^{1/7} \cdot (1 + 0.22Cc^2) \tag{13}$$

where e_a is the atmospheric water vapor pressure (kPa) and T_a is the air temperature (K). e_a is computed with the air's relative humidity and temperature.

2.4.1.3 Turbulent heat fluxes

Sensible and latent heat fluxes Q_h and Q_l are computed using the bulk aerodynamic method (Kustas et al., 1994):

$$Q_h = \rho_a c_a C_h V (T_a - T_t^n) \tag{14}$$

$$Q_l = l_v . \frac{0.622\, \rho_a}{P_a} C_h V (e_a - e_t^n) \tag{15}$$

where ρ_a is the air density (kg m^{-3}), c_a is air-specific heat (J kg^{-1}K^{-1}), V is the wind velocity (m s^{-1}), T_a and T_t^n are the air and snow surface temperature (K), l_v is the water latent heat of vaporization or sublimation (J kg^{-1}), P_a is the atmospheric pressure (kPa) and e_a is the water vapor pressure in the air (kPa). The saturation vapor pressure e_t^n (kPa) is calculated at the snow surface temperature. The bulk coefficient C_h is adapted from the bulk coefficient in neutral atmospheric conditions C_{hn} depending on the atmospheric stability conditions as follows:

$$\begin{array}{lll} C_h = & C_{hn}(1 - 16\, R_i)^{0.75} & if\ R_i \leq 0 \\ C_h = & \dfrac{C_{hn}}{1 + k_{tur} \frac{R_i}{0.2}} & if\ 0 < R_i \leq 0.2 \\ C_h = & \dfrac{C_{hn}}{1 + k_{tur}} & if\ 0.2 < R_i \end{array} \tag{16}$$

where R_i is the bulk Richardson number and k_{tur} is a coefficient detailed below. C_{hn} is computed as:

$$C_{hn} = k^2(\ln\left(\frac{z_a}{z_0}\right))^{-2} \tag{17}$$

where k is the Von Karmin constant, z_a is the measurement height of air temperature and wind speed (m) and z_0 is the snow surface roughness whose value typically ranges between 5.10^{-4} and 5.10^{-3} meters (Dingman, 2002). The value for z_0 is set during the model parameterization.

The bulk Richardson number R_i (American Meteorological Society, 2012) is used to assess the atmospheric stability conditions:

$$R_i = \frac{2gz_a(T_a - T_t^n)}{(T_a + T_t^n)V^2} \tag{18}$$

where g is gravity acceleration (m s^{-2}). For values of R_i above 0.2, it is generally assumed that the turbulent heat fluxes no longer exist because of the atmospheric stability conditions. Brun et al. (1989) showed that this assumption tends to heavily underestimate the heat balance of the snowpack as heat conduction and vapor diffusion between the air and the snowpack surface still occur. The parameter k_{tur} was therefore introduced in order to account for the heat exchanges between the air and the snowpack surface when the atmospheric conditions are stable. k_{tur} is set during the model parameterization.

2.4.1.4 Liquid water input

Liquid water inputs are caused by percolation from the upper layer or by rain, in the case of the top layer. Liquid water inputs can result in sensible heat flux if the water and snow temperatures are different and in latent heat flux if a phase change occurs. Percolating water is supposed to be at 0°C, while rain water temperature equals the air temperature. If the water temperature is above 0°C, it will first cool down to 0°C, and thus release sensible heat:

$$Q_{w,s} = \mathrm{c}_w \rho_w T_r R \tag{19}$$

where c_w is the water-specific heat (J kg^{-1} K^{-1}), ρ_w is the water density (kg m^{-3}), T_r is the water temperature (K), and R is the water input intensity (m s^{-1}). If the snow temperature is below 0°C, liquid water can partially or completely freeze, thus releasing latent heat up to a value of:

$$Q_{w,l} = l_f \rho_w R \tag{20}$$

where l_f is in J kg^{-1}.

2.4.1.5 Conduction fluxes

The conduction flux Q_c between a layer i and the adjacent layers i-1 and i+1 can be described using the Fourier conduction formula (DeWalle and Rango, 2008), as shown in equation 21:

$$Q_c = \frac{T_t^{i-1} - T_t^i}{\frac{H_t^{i-1}}{2k_t^{i-1}} + \frac{H_t^i}{2k_t^i}} + \frac{T_t^{i+1} - T_t^i}{\frac{H_t^{i+1}}{2k_t^{i+1}} + \frac{H_t^i}{2k_t^i}} \tag{21}$$

where T, H and k are the temperature, height and thermal conductivity of each layer, respectively. The thermal conductivity of snow is computed using the formula proposed by Yen (1981):

$$k_t^i = k_g \left(\frac{\rho_t^i}{\rho_g}\right)^{1.88} \tag{22}$$

where the subscript g refers to ice and k and ρ are thermal conductivity (W m^{-1} K^{-1}) and density (kg m^{-3}), respectively.

Since applying the Fourier conduction formula to the conduction heat flux between the base of the snowpack and the ground would require having access to soil thermal characteristics data and because variations in soil thermal properties during the winter are generally low in comparison to the other terms of the energy budget (Gray and Male, 1981), a decision was made to consider heat exchange at the ground/snow interface as a constant flux toward the snowpack:

$$Q_g = \ Q_{ground \rightarrow pack} \tag{23}$$

where $Q_{ground \rightarrow pack}$ is a positive value that is set during model parameterization.

2.4.2 Mass balance of the layer

Once the internal energy variation of the layer is obtained, equation 10 is used to compute the new temperature of the layer T_{t+1}^i without considering any phase changes. T_{t+1}^i can thus be expressed as follows:

$$T_{t+1}^{i} = \frac{Q^{i}\Delta t}{c_t^i \rho_t^i H_t^i} + T_t^i \tag{24}$$

The heat capacity of snow c_t^i is computed as the weighted sum of the heat capacity of ice, water and air (Armstrong and Brun, 2008):

$$c_t^i = \frac{1}{\rho_t^i H_t^i}\left(\rho_g H_g c_g + \rho_w H_w c_w + \rho_a H_a c_a\right) \tag{25}$$

where the subscripts g, w and a represent ice, water and air, respectively, and H, ρ and c are the equivalent height, density and specific heat of each component, respectively. The equivalent heights are:

$$\begin{aligned} H_g &= SWE_t^i - LW_t^i \\ H_w &= LW_t^i \\ H_a &= H_t^i - SWE_t^i \end{aligned} \tag{26}$$

The specific heat of ice is adjusted, depending on the temperature of the layer (Dorsey, 1968):

$$c_g = 7.8\, T_t^i + c_{g,0} \tag{27}$$

where $c_{g,0}$ is the ice-specific heat at 0°C, and equals 2115 J kg^{-1} K^{-1}.

The different situations which can occur at this point, depending on T_t^i and T_{t+1}^i values, are detailed below. If either T_t^i or T_{t+1}^i is different from 0°C, no melt occurs. Melt is considered as occurring only when both T_t^i and T_{t+1}^i are equal to 0°C. In this case, $\Delta T^i =$

0 and equation 10 is used to compute the new liquid water content of the layer LW_{t+1}^{i} as follows:

$$LW_{t+1}^{i} = \frac{Q^{i}\Delta t}{l_f \rho_w} + LW_t^{i} \tag{28}$$

The difference between LW_{t+1}^{i} and LW_t^{i} represents the water equivalent of melted snow or refrozen water M_t^{i}. If M_t^{i} has a negative value, it means that a certain amount of liquid water has frozen and released latent heat, thus maintaining the temperature of the layer at 0°C. If M_t^{i} is greater than the water equivalent of the layer, it means that the layer melts completely. Otherwise, the new liquid water content LW_{t+1}^{i} is compared to the water holding capacity of the layer $LWHC_t^{i}$. The latter represents the maximum amount of liquid water that can be retained against gravity, and is expressed as a percentage of the volume of void of the layer, as shown in equation 29:

$$LWHC_t^{i} = k_{LWHC}\,(H_t^{i} - \left(SWE_t^{i} - LW_t^{i}\right)\frac{\rho_w}{\rho_g}) \tag{29}$$

where k_{LWHC} is a percentage between 5 and 10% and the rest of the right-hand side of the equation is the volume of void, where ρ_g is the density of ice. The value of k_{LWHC} is set during the parameterization step.

If LW_{t+1}^{i} is greater than $LWHC_t^{i}$, LW_{t+1}^{i} is set to $LWHC_t^{i}$ and excess liquid water is integrally transmitted to the layer below, provided it can accept further liquid water inputs. The new height of the layer after melt has occurred, $H_{t'}^{i}$, is computed following equation 30:

$$H_{t\prime}^{i} = H_{t}^{i} - M_{t}^{i} \frac{\rho_w}{\rho_t^i} \tag{30}$$

2.4.3 Settling

Settling is assessed in terms of height decrease. The final height of the layer H_{t+1}^{i} is computed from $H_{t\prime}^{i}$ following equation 31, which was built by combining different existing formulations:

$$H_{t+1}^{i} = H_{t\prime}^{i} \frac{1 - \frac{\sigma}{\eta_t^i} \Delta t}{1 + K_d \mathrm{e}^{0.04\, T_t^i - 0.05\, \max(\rho_t^i - \rho_{s,meta,max}, 0)} \Delta t} \tag{31}$$

The numerator represents the effects of the weight of the upper layers as computed by Navarre (1975). σ is the weight of the overlying layers (Pa) and η_t^i is the viscosity of the layer (Pa s). The viscosity is computed following the equation of Gubler (1994):

$$\eta_t^i = 1.86\ 10^{-6} \cdot \mathrm{e}^{0.02\, \rho_t^i + \frac{1800}{T_t^i}} \tag{32}$$

where ρ_t^i and T_t^i are the snow density and temperature.

The pressure sustained by the layer i in an n layers pack is:

$$\sigma_t^i = \frac{g}{1000} \sum_{j=i+1}^{n} (SWE_t^j\, \rho_w) \tag{33}$$

The denominator of equation 31 represents the effects of destructive metamorphism, and is adapted from Anderson (1976). Destructive metamorphism occurs when the layer is young, and is assumed to be negligible when the density reaches the threshold

$\rho_{s,meta,max}$. The coefficient K_d represents the hourly settling rate when $T_s = 0°C$ and $\rho_t^i < \rho_{s,meta,max}$. The values for K_d and $\rho_{s,meta,max}$ are set during model parameterization. The new density of the layer is then computed:

$$\rho_{t+1}^i = SWE_{t+1}^i \frac{\rho_w}{H_{t+1}^i} \tag{34}$$

where ρ_w is the water density.

2.5 New snow handling

At the end of each hour, prospective snow precipitation is added to the snowpack. New snow characteristics are computed as follows. The snow temperature is set to the air temperature. New snow density ρ_s is computed depending on the air temperature (Anderson, 1976):

$$\begin{aligned} \rho_s &= \rho_{ns} && \text{if } T_a < T_{\rho_{ns}} \\ \rho_s &= \rho_{ns} + 1.7(T_a - T_{\rho_{ns}})^{1,5} && \text{else} \end{aligned} \tag{35}$$

where ρ_{ns} is the density of new snow if the air temperature T_a is below the threshold $T_{\rho_{ns}}$. The values for ρ_{ns} and $T_{\rho_{ns}}$ are set during model parameterization. The total height of added snow H_{as} is computed from the water equivalent of the precipitation using equation 34. The number of new layers added to the snowpack is the integer part of $\frac{H_{as}}{H_{min}}$, where H_{min} is the minimum height of a layer, set to 1 cm. We consider that new snow does not contain any liquid water when it is added to the pack.

2.6 Layers management

In order to keep the number of layers reasonably low computer-wise, while still matching the real layering of the snowpack, MASiN layers are managed dynamically at the end of each hour. Two thickness thresholds are set for that purpose, a minimum and a maximum. The minimum thickness is set to 1 cm for all the layers in order to ensure the stability of the iterative scheme. If the layer is too thin, energy exchanges can be misestimated. That can also be the case if a layer is too thick; a maximum thickness was thus set, with a value of 2 cm for the top fifteen layers, and 4 cm for the rest of the pack. As most energy exchanges occur at or near the pack surface, it is necessary to have a finer spatial discretization than in the rest of the pack. When a layer reaches the minimum thickness, it is merged with the thinnest adjacent layer. If the newly created layer exceeds the maximum thickness, it is separated into two layers with similar properties. The maximum number of layers is set to 70 to keep the computation time moderate. After new layers are added to the pack, a test is conducted to check if the maximum number of layers has been reached. If it has been exceeded, adjacent layers are combined according to the following rules: no combination of layers which have an age difference of more than 2 days is allowed, and no new layer having a thickness exceeding the maximum thickness will be created. If no combination is possible using these rules, the age threshold is increased by one day, and the combination test is run until the number of layers is below the maximum value.

2.7 Parameterization of the model

The parameterization was performed for one study site only, and the parameters were left unchanged for the rest of the study. A two-step protocol was followed. First, a sensitivity analysis was performed to assess the influence of the 18 model parameters on the model output. Parameters with little or no influence were set to values based on the literature, while the remaining parameters were adjusted by calibration at the parameterization site.

Parameterization was performed for the Dorval site (45.47°, -73.74°) near Montreal, Quebec, Canada. Dorval was selected based on the quality of the dataset it offers and because of its central position among the different sites where MASiN is tested in this study. The sensitivity analysis was performed over a ten-year period and calibration was done on the first five years of this period.

The normalized root mean square error was used for the sensitivity analysis to compare the height modeled with a value of the parameter and the height modeled with a literature-based value of the parameter. For each parameter, ten values spreading between two bounds selected based on published values, were tested. The effect of each parameter was assessed separately.

Sensitivity analysis outputs showed that the conduction heat flux between the ground and the snowpack $Q_{ground \to pack}$ is the parameter with the most influence on the modeled snow depth. The solar radiation absorption coefficients β_{dir} and β_{dif}, as well as the minimum and maximum fraction of direct solar radiations $k_{dir,min}$ and $k_{dir,max}$, have a very limited influence, and were therefore set to values from the literature. The minimal albedo for direct radiations $a_{dir,min}$ will not be adjusted either, as its influence is minimal. The daily temperature range threshold ΔT_{Ccmin} is less influential than ΔT_{Ccmax}, but a decision was made to compute both of them, as explained in section 2.3.2.2.

All the other parameters were adjusted using the SCEUA algorithm (Duan et al., 1993a) with the Nash Sutcliffe coefficient (Nash and Sutcliffe, 1970) used as the objective function. A single calibration sequence was performed, which gave a value of 0.79 for the Nash Sutcliffe coefficient. The final parameterization is presented in Table 1.

Table 1 Final parameterization of the model.

Parameter (unit)	Value	Source
$\rho_{s,meta,max}$ (kg m^{-3})	200	Adjusted to Dorval conditions
$a_{dir,min}$	0.45	Anderson (1976)
$a_{dif,min}$	0.35	Anderson (1976)
ρ_{ns} (kg m^{-3})	80	Adjusted to Dorval conditions
k_{LWHC} (%)	8	Adjusted to Dorval conditions
K_d (h^{-1})	0.01	Adjusted to Dorval conditions
β_{dir} (cm^{-1})	0.4	Armstrong and Brun (2008)
β_{dif} (cm^{-1})	4	Armstrong and Brun (2008)
$Q_{ground\rightarrow pack}$ (W m^{-2})	10	Adjusted to Dorval conditions
$T_{\rho_{ns}}$ (°C)	-15	Adjusted to Dorval conditions
ΔT_{Ccmin} (°C)	Equation 4	Adjusted to Dorval conditions
ΔT_{Ccmax} (°C)	Equation 5	Adjusted to Dorval conditions
k_{SWmin}	0.2	Adjusted to Dorval conditions
k_{SWmax}	0.75	Adjusted to Dorval conditions
$k_{dir,min}$	0.35	Linacre (1992)
$k_{dir,max}$	0.85	Linacre (1992)
z_0 (m)	0.0015	Adjusted to Dorval conditions
k_{tur}	4	Adjusted to Dorval conditions

3. Study site, comparative models and performance assessment criteria

3.1. Study sites

Twenty-three sites across Canada and Sweden were chosen to assess the ability of MASiN to simulate the evolution of the snow cover in various environments. The sites were selected in order to represent different climate zones. They were sorted into 5 groups based on geographical criteria, as shown in Fig. 2.

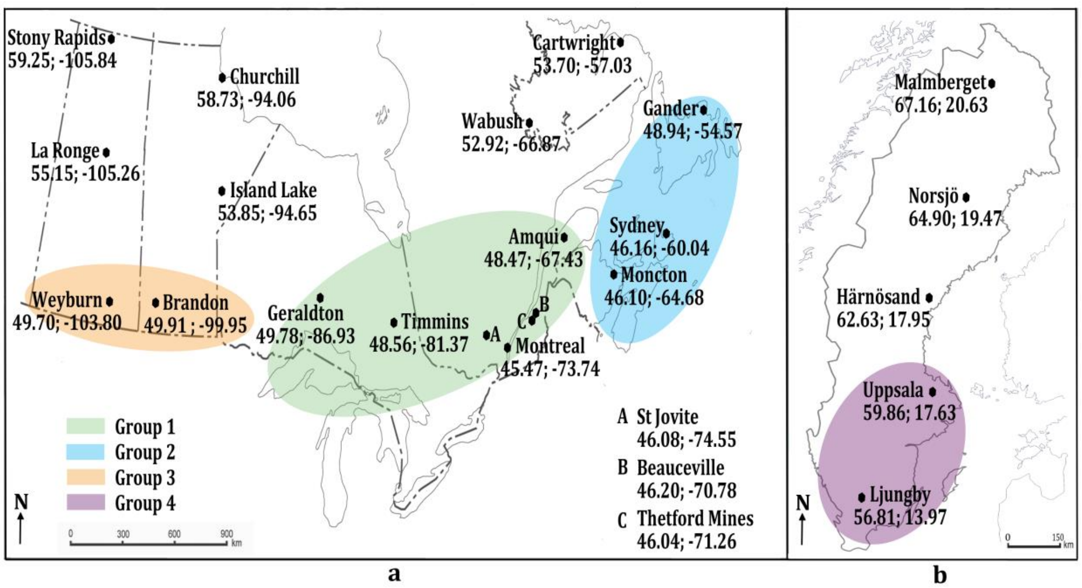

Fig. 2. Locations of the 23 sites in Canada (a) and Sweden (b). Groups 1 to 4 are highlighted on the map and group 5 consists of the nine remaining sites.

Group 1 is comprised of five sites in Quebec and two in Ontario. Group 2 is composed of three sites on the Canadian East coast that have similar latitudes as the parameterization site, but are subject to strong oceanic influence. Group 3 is made up of two sites in southern Manitoba and Saskatchewan, which represent typical continental climate, at a latitude comparable to that of Dorval. Group 4 is comprised of the two Swedish sites with the lowest latitudes, representing more temperate climate. Group 5 includes the nine high latitude sites, which are characterized by latitudes greater than 53° in Canada and greater than 60° in Sweden. Those sites were chosen to account for continental climate at high latitudes in Canada, some with possible oceanic influences, and conditions close to sub-polar climate in Sweden. All the sites are located in plain terrain.

For each station, data have been selected based on the availability of all needed measurements and on the quality of the time series data. Required measurements are the air temperature, relative humidity, wind speed and direction at an hourly time step as well as precipitations and SD at a daily time step. Winters (here defined as the 1-10 to 31-05 period) with more than 35 gaps in one or several measurements or with gaps that were not possible to correct or replace based on other measurements, have been rejected from the analysis. Table 2 presents the results of data selection. Days with corrected values represent on average 1.1% of the winter days used in the analysis.

Table 2. Description of the time series data. The "# of rejected winters" corresponds to the number of winters between the start and the end years that have been removed from the time series for quality reasons. "Corrections (%)" represents the percentage of winter days with at least one corrected parameter.

Station	Start year	End year	# of rejected winters	Corrections (%)
Dorval	2003	2014	0	5.1
St-Jovite	1994	2008	1	1.3
Beauceville	1997	2015	0	2.5
Geraldton	1983	2014	0	0.2

Amqui	1995	2014	4	8.2
Timmins	1989	2009	2	0
Thelford Mines	2006	2015	0	0.8
Sydney	1984	2014	2	0.5
Moncton	1993	2012	1	0
Gander	1981	2011	2	0
Brandon	1993	2012	0	0.5
Weyburn	1994	2008	1	0.5
Uppsala	1986	2003	2	0
Ljungby	1995	2015	0	0
Hamosand	1992	2015	0	0.3
La Ronge	1982	2012	2	1.3
Island Lake	1986	2014	1	0
Churchill	1978	1998	1	0.1
Stony Rapids	1987	2009	1	0.6
Norsjö	1997	2015	1	3.5
Malmberget	1997	2015	1	0
Wabush	1982	2012	1	0.4
Cartwright	1984	2014	1	0.3

Differences in seasonal evolution of the snow cover between the groups were verified using two indicators: the annual maximum uninterrupted snowpack presence, calculated as the maximum number of days during which snow is continuously present on the ground each year, and the annual maximum snow depth. These two indicators were computed over periods ranging from nine to thirty-one years, depending on data availability at each site. Results are presented in Fig. 3.

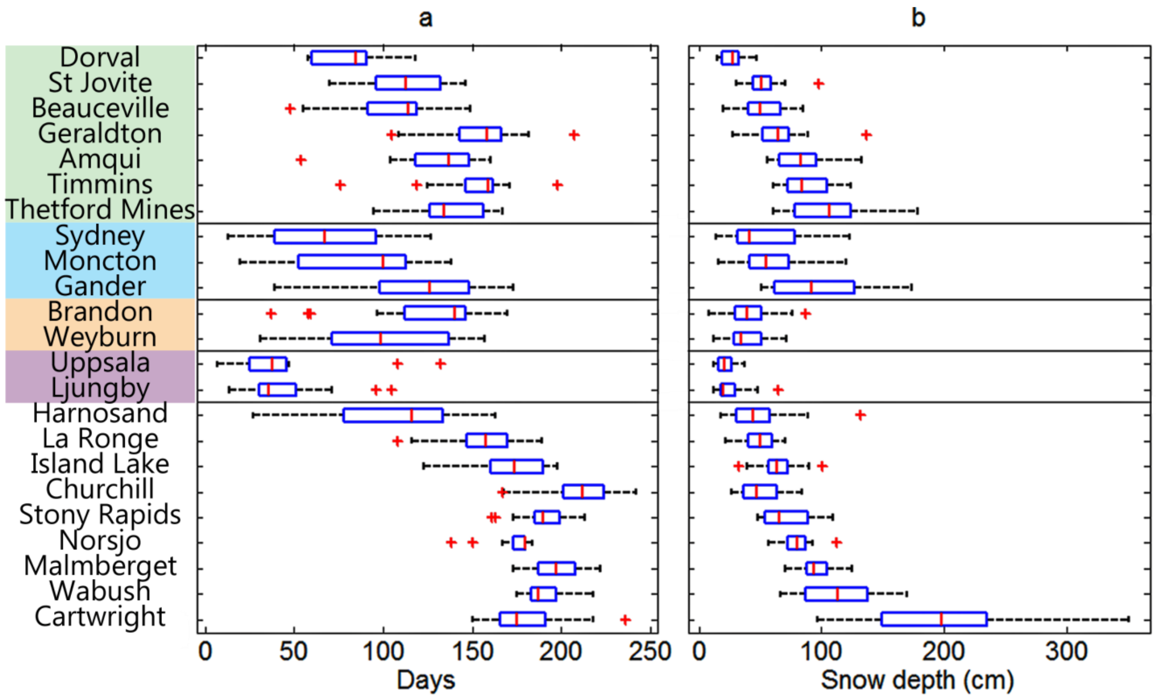

Fig. 3. (a) Maximum uninterrupted snowpack presence and (b) maximum annual snow depth at each site. Groups are identified by the same color code as in Fig. 2. The red line indicates the median value; left and right edges of the boxes indicate the 25th and 75th percentiles, respectively; left and right whiskers define the non-outlier range. Outliers are plotted as red crosses.

Despite their relative proximity, sites from Group 1 present a wide range of snow cover evolution, with some sites like Dorval presenting low maximal snow depth and short continuous snowpack presence, and others, such as Thetford Mines, showing significant snow accumulation and duration. Inter-annual variability of the two criteria is also inconsistent between the sites. Sites from Group 2 are characterized by significant variations of both maximum annual snow depth and maximum uninterrupted snowpack presence over the years. Sites from Group 3 have similar maximal snow depth distribution, but Weyburn exhibits huge variability of continuous snowpack presence. Group 4 is composed of the two sites having the lowest maximum annual snow depth and maximum uninterrupted snowpack presence, and represent typical mid-northern Europe conditions, as expected. Sites in Group 5 have a varying maximal snow depth variability and continuous snow cover presence, but on average, they are the sites with the maximum uninterrupted snow presence. Harnosand is the exception, with distribution of both criteria closer to that of Weyburn. Fig. 3 confirms that the sites selected for the study expose MASiN to a wide range of conditions and seasonal snowpack characteristics.

3.2. Comparative models

MASiN was compared with three snow models: two empirical (named Model C and Model D for the purpose of this study), and one mixed degree day/energy balance model named Hydrotel. These three models run at a daily time step. The two empirical snow models both have proven abilities to reproduce snow height with good accuracy once calibrated for a given site.

Model C (Farbrot and Hanssen-Bauer, 2009) requires daily total precipitation P_{tot} and daily mean temperature T_{av} to compute snow height S_n with five calibrated parameters (a, b, c, d and e), as shown in equation 36:

$$\begin{array}{lll} S_n = & S_{n-1} + bT_{av} & if\ (T_{av} - a) > 0 \\ S_n = & S_{n-1} + cP_{tot} + dT_{av} + e & if\ (T_{av} - a) \leq 0 \end{array} \qquad (36)$$

Model D (Baraer et al., 2010) requires daily solid precipitation P_s and daily maximum temperature T_{max} to compute snow height S_n with three calibrated parameters (a, b and c), as shown in equation 37:

$$S_n = S_{n-1} + bP_s - a(\max(T_{max}, 0))^c \tag{37}$$

Hydrotel is a widely used hydrological model whose performances have been assessed at several sites across Quebec. Its snow module was chosen for its ability to simulate snow height as well as other variables relevant for hydrological purposes. It requires daily minimum and maximum temperatures and total or separated daily precipitation. It is much closer to MASiN in terms of complexity, and is thus expected to provide similar performances. It relies on a mixed degree day/energy balance method to compute the snow height evolution, which means that most of the components of the energy balance are computed using a form of degree day equation. It uses five calibrated parameters. Further information can be found in Turcotte et al. (2007).

The three reference models were first used in similar conditions as MASiN. They were calibrated against snow height measurements at the Dorval site and applied to the 22 other sites using a unique set of parameters. In order to further challenge MASiN's robustness, the three reference models were then calibrated at each site with the first half of the data and validated on the entire dataset. The calibration was conducted using the SCEUA algorithm (Duan et al., 1993b) following the recommendations of Arsenault et al. (2014), by selecting the best set of parameters out of ten calibration sequences per site, using random initial search parameters. The Nash Sutcliffe coefficient was used as the objective function. Its values on the calibration periods range between 0.67 and 0.96, with a mean value of approximately 0.82 for the models taken together.

3.3. Performance assessment and comparison criteria

Three criteria were used in order to have both an insight on the raw performance of each model and a more detailed vision of the ability of each to provide simulations that are accurate time-wise. In terms of hydrology, and especially in reservoir management, being able to time the moment when water is released is crucial.

The Nash-Sutcliffe coefficient gives a general overview of the agreement between the simulated and measured snow depths. One value is computed for each model at each site.

The “wrongly simulated state” represents the number of times the simulated snowpack is erroneously present or absent. It is expressed as a percentage of the number of days of presence of the real snowpack. It denotes the ability of the model to correctly simulate events of complete melt during the winter or events of small snow accumulation at the beginning or the end of the season. One value is computed for each model at each site. The best value that can be obtained for this criterion is 0%.

The “melt offset” characterizes the ability of the models to predict the time of spring snowpack vanishing. It is corresponds to the mean of the absolute yearly difference in the number of days between the disappearance of the simulated and observed snowpacks. The disappearance date is assumed to be the time when the observed pack has lost 95% of its maximum height. The value aimed for this criterion is 0 days. All three criteria are calculated on daily basis.

4. Results and discussion

4.1. Model calibration and validation at the Dorval site

All models were calibrated on the winters of years 2003 to 2008 and validated on the winters of years 2009 to 2014 at the Dorval site. Calibration provided good Nash-Sutcliffe coefficients for all the models. Model D and Hydrotel exhibited the best calibration results followed by MASiN and Model C. As expected, results from validation are inferior to the ones obtained during calibration for all models. Model C shows the lowest Nash-Sutcliffe coefficient during validation and MASiN displays the highest. Hydrotel and Model D show comparable results in validation.

Table 3. Nash-Sutcliffe coefficients resulting from the models' calibration and validation at the Dorval site.

Model	Calibration	Validation
MASiN	0.79	0.76
Hydrotel	0.84	0.70
Model D	0.86	0.71
Model C	0.80	0.56

Fig. 4. Provides an example of simulation results for three winters in the validation period. The winter 2013-2014 corresponds to the best simulation results for the MASiN model and, at the same time, is characterized by numerous fluctuations of the SD. The other two years are also displayed to get a sense of the variability in skill from one winter to the next. For the 2013-2014 year, MASiN differentiates itself from reference models

by being able to reproduce multiple fluctuations in a successful way. None of the models predict the exact day of snowpack vanishing. For the other years, it can be seen that there are some snow events that are less successfully modeled by MASiN, although that is also the case with the other tested snow models.

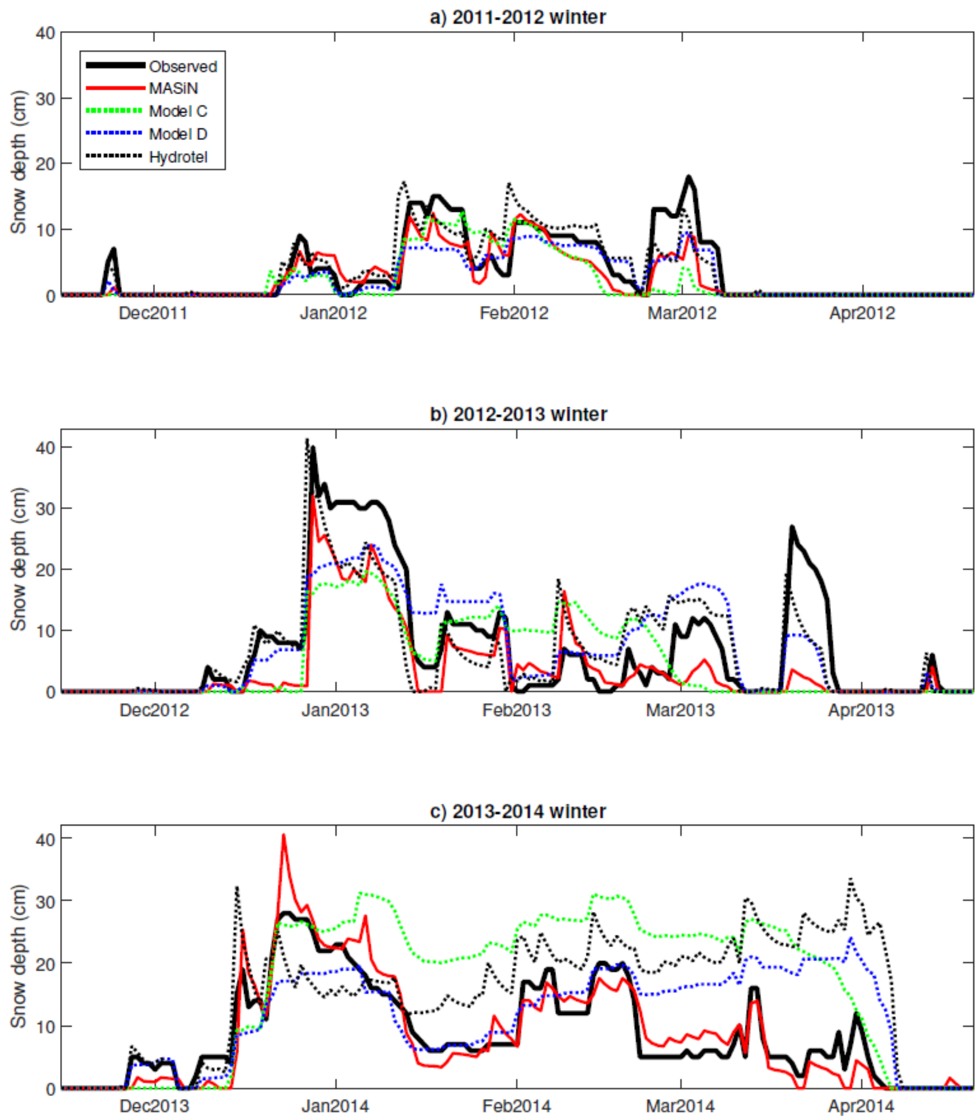

Fig. 4. Observed and simulated snow depth at Dorval for winters a) 2011-2012, b) 2012-2013 and c) 2013-2014.

4.2. Multisite general performances

The model performances were first assessed using MASiN and the three reference models in similar conditions: one calibration performed at Dorval followed by applications to 22 other sites keeping the set of parameters intact. Fig. 5 shows simulation results using the entire datasets for each site.

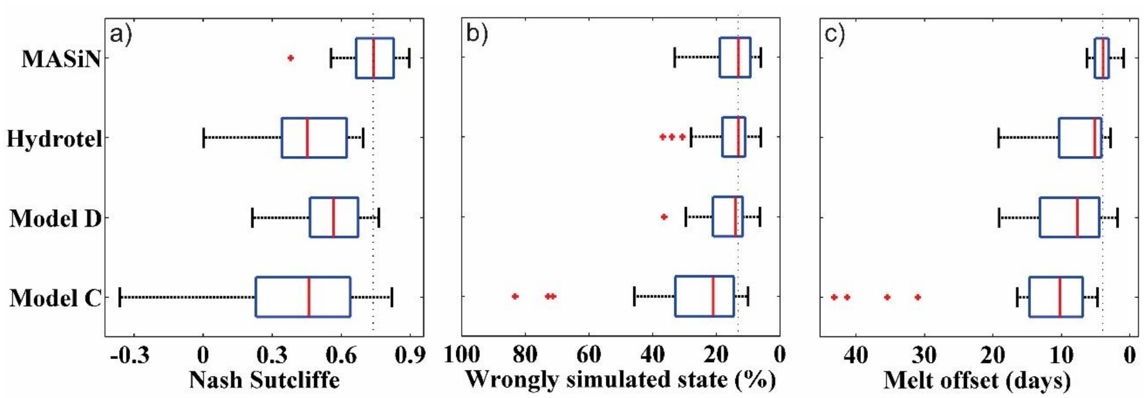

Fig. 5. Assessment criteria for the four models used in similar conditions at the 23 sites. (a) Nash Sutcliffe coefficient (b) Melt offset (c) Wrongly simulated state. Vertical black lines indicate MASiN's median value. Wrongly simulated state and melt offset axes are reversed to facilitate interpretations.

With the exception of one outliner at 0.38 in Fig 5a, MASiN provides consistent and reasonably high Nash Sutcliffe coefficients at the different sites. With a median Nash Sutcliffe coefficient of 0.74, MASiN shows an overall higher performance than other models used in similar conditions. Model D (0.57) Model C and Hydrotel (0.46) present both inferior medians and wider distributions. The difference between MASiN and the other models is less contrasted regarding the wrongly simulated state. Hydrotel, Model D and MASiN have comparable medians (around 13%) and distributions. Model C shows lower performances with a median over 20% and a wider distribution.

MASiN's results for the melt offset criteria are very contrasting from the reference models. MASiN's median reaches 3.9 days on 23 sites while Hydrotel, Model D and Model C reach 5.2, 7.7 and 10.2 respectively. As is the case for the Nash Sutcliffe coefficient, MASiN has the tightest melt offset distribution of the four models.

Overall, MASiN shows comparable (wrongly simulated state) to substantially higher (Nash Sutcliffe and melt offset criteria) performances than those of the reference models. MASiN demonstrated a high level of robustness by reproducing SD with a consistent accuracy over the 23 study sites. The situation is different for the reference models that all show clear limitations in performing at different sites with a unique set of parameters. Among the reference models, Model C is the one showing the worse robustness, followed by Hydrotel and Model D.

4.3. Multisite detailed performance

In order to identify MASiN's strengths and weaknesses in the context of a multisite application, the model's results are compared here to reference models calibrated at each study site. Analyzing the performance of MASiN for each group of sites in such conditions is required to assess if the model accuracy is site-group related. Results for each site are presented in Fig. 6.

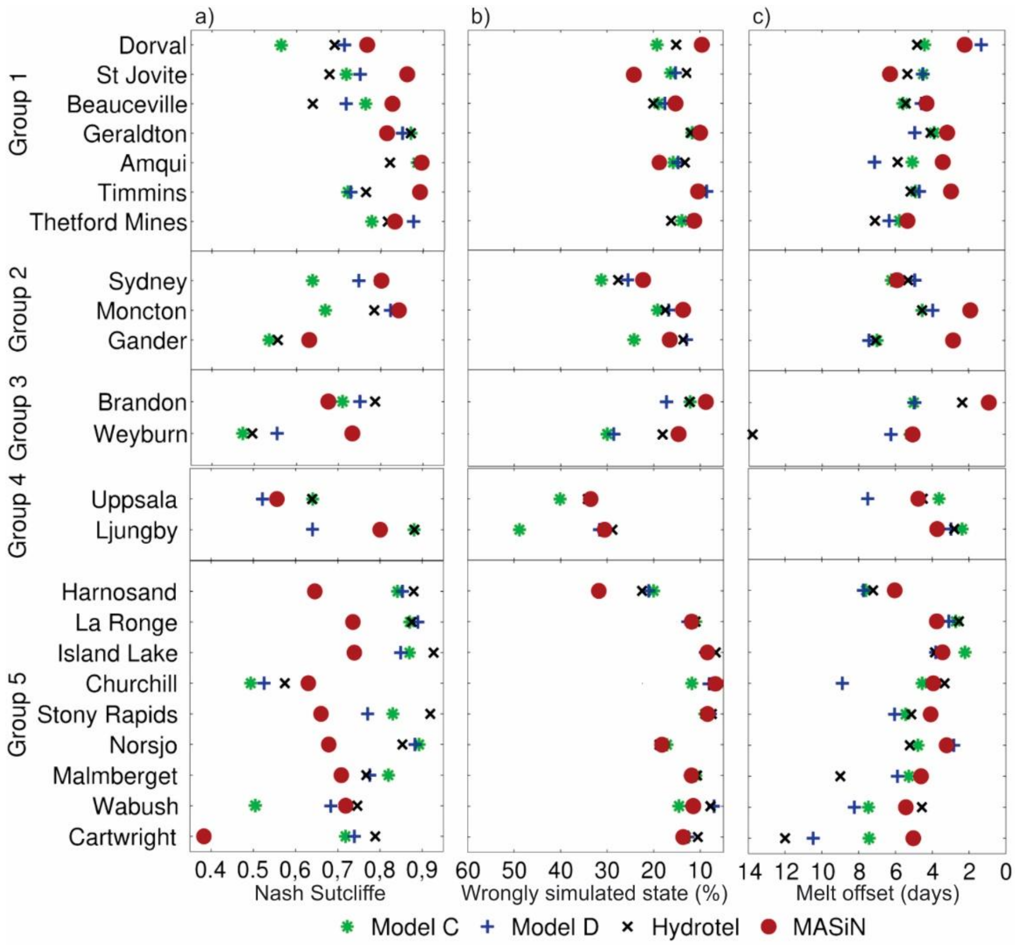

Fig. 6. Results for the five groups of study sites. MASiN, used with a unique set of parameters, is here compared with reference models calibrated at each site. The left panel (a) shows the Nash Sutcliffe coefficient, the center panel (b) presents the wrongly simulated state and the right panel (c) shows the melt offset. Wrongly simulated state and melt offset axes are reversed to facilitate interpretation.

Group 1

With respect to the Nash Sutcliffe coefficient, MASiN shows the best performance at five out of seven sites. At the remaining two sites, the performance is still very good, with NSE values close to 0.8. MASiN has the best performance at four out of seven sites in terms of the wrongly simulated state, with only one poor value at St-Jovite. MASiN shows the best performances for the melt offset at five out of seven sites. The performance at St-Jovite is also poor for this criterion. Overall MASiN can be seen as the best performer for this group which hosts the parameterization site.

Group 2

MASiN has the best performance in terms of the Nash Sutcliffe coefficient, with values above 0.8 at the Sydney and Moncton sites, and a value of 0.63 at the Gander site, where the four models show their worst performance. Model D and Hydrotel are quite close to MASiN at each site. The performance of Model C is substantially inferior. Regarding the wrongly simulated state, Model D, Hydrotel and MASiN exhibit comparable performances with values ranging from 13% to 28%. The performance of Model C is here again substantially inferior for this criterion. Each model experiences its worst performance in Sydney, where the annual maximum snow depth and the continuous snow cover presence are the smallest of the three sites (see Fig. 3.). The situation for the melt offset shows comparable performances for Model C, Model D and Hydrotel. MASiN shows better performances at two of the three sites, and a comparable performance at the Sydney site. As for group 1, MASiN seems to show the overall best performance in Group 2.

Group 3

MASiN shows the best performance for the wrongly simulated state and the melt offset at each site, and has the best Nash Sutcliffe coefficient at Weyburn. The MASiN Nash Sutcliffe coefficient for Brandon can be still considered good (0.68), but it is lower than for the three other models, which exhibit good performances for that criterion. MASiN could also be considered among the best models for this group, keeping in mind that it was not calibrated at each site contrarily to the other models.

Group 4

Results for Group 4 are more contrasted than for the first three groups. MASiN shows the best performance for only one criterion at one site, and the value is still poor (Uppsala, wrongly simulated state of 33%). Nash Sutcliffe values at Uppsala are poor for all models, whereas there are some very good performances at Ljungby. The wrongly simulated state is very poor for all the models at each site. Melt offset values are satisfactory overall; at least two models perform better than MASiN at each site.

Group 5

MASiN has the worst performance at seven out of nine sites in terms of the Nash Sutcliffe coefficient, with values ranging between 0.64 and 0.74, and Cartwright being the exception with a very low value of 0.38. MASiN is or is close to being the best model at the two remaining sites. The performances of the four models in terms of the wrongly simulated state are very close at each site. Performances in terms of the melt offset vary from one site to another. Overall MASiN clearly shows the poorest performance for Group 5.

MASiN shows very good overall performances at sites from Groups 1, 2 and 3, and despite a few counter-performances, it can be rated the best model for these groups. For Groups 4 and 5, MASiN exhibits poorer overall performances and less dominance over the comparison models, showing limits in the model robustness.

4.4. Discussion

A detailed analysis of the results shows that MASiN's performance varies from one group of sites to another.

Of the ten best performances of MASiN with respect to the Nash Sutcliffe coefficient, nine are seen at sites in Groups 1 and 2. At all of these sites, the wrongly simulated state is close to or below 20% (with only one exception) and the maximum melt offset is 6 days. Sites in Groups 1 and 2 are the closest sites to Dorval, where the parameterization of MASiN was performed. At sites in Group 2, the comparison models exhibit poorer overall performances than for Group 1. Sites in Group 2 are characterized by great inter-annual variability of both continuous snowpack presence and maximum snow depth (see Fig. 3). Because of calibration, reference models may have difficulty showing consistent performances when winter conditions vary, thus possibly explaining why only MASiN shows stronger performances at Group 2 sites.

MASiN can be seen as the best model at sites in Group 3 despite not performing as well as for Groups 1 and 2. Sites from Group 3 are located further from Dorval and the difference in climatic conditions can explain the performance decrease seen with them. However, results from Groups 1, 2 and 3 tend to show that the physical basis of MASiN allows strong transferability in both space and time.

Performances for Group 4 are variable. The main similarity in performance between the models is seen with the wrongly simulated state, which is very poor at the two sites. The specificity of Group 4 lies in very short continuous snowpack presence and low snow accumulation. At the sites in that group, several accumulation and melt periods occur during a single winter season. Poor wrongly simulated state performance indicates that all models have trouble representing these repeated appearances and disappearances of the snowpack. However, as the snow height at these sites is relatively low, differences between measured and simulated snow depth remain small, even when the presence is wrongly simulated, causing the Nash Sutcliffe coefficient to remain relatively high.

At sites in Group 5, MASiN shows performances comparable to those in Group 1 in terms of the wrongly simulated state and melt offset. The two main differences with Group 1 are that (1) the other models show very strong overall performances for the three criteria, and (2) Nash Sutcliffe coefficients for MASiN are smaller. Except for Harnosand, sites in Group 5 are characterized by a long continuous winter presence and a relatively low inter-annual variability of both maximum snow depth and continuous snow presence. These conditions can be favorable to calibration efficiency, thus possibly explaining the strong performances of the reference models at these sites. This hypothesis does not however apply to Churchill, where the poor Nash Sutcliffe performances of all models remain unexplained. Besides the good performances of the comparison models, MASiN shows a weaker Nash Sutcliffe performance for Group 5 sites than for the other groups. After comparing the measured snow depth with the MASiN simulated snow depth, it appears that at the sites in Group 5, the snow depth is heavily underestimated by MASiN because of both misestimated new snow density and overestimated densification. This results in depth differences of up to 50%. The overestimation of density also makes for a faster ripening of the snowpack as conduction fluxes, absorbed shortwave radiations, and liquid water transmission are overestimated.

Sites in Group 5 represent very specific climatic conditions that are different from those around the parameterization site, thus making the used parameters less suited to the characteristics of that group. This shows that despite the seeming robustness of MASiN, there are still limits to the areal extent validity of its utilization under the conditions imposed by the present study. However, the results so far do not allow a differentiation between parameterization and design limits. For instance, some of the equations chosen during MASiN's design were developed and validated at specific sites. Their tuning capacity through the adjustment of their parameters is therefore limited to a certain range of validity. New snow density, for example, is computed with a relationship based on measurements from Alta, Utah (Anderson, 1976), where climatic conditions may differ from those of Group 5 sites.

5. Conclusion

The non-data intensive physically based model MASiN computes the energy and mass balance of multiple layers of the snowpack using hourly air temperature, relative humidity and wind speeds, as well as daily precipitations. The model targets high robustness and limited calibration requirements for multisite applications. In order to assess MASiN's robustness a unique parameterization phase was conducted at one site (Dorval) and parameters were kept unchanged for different study sites. MASiN's performance was then compared to those of three reference snow models at 23 point locations across Canada and Sweden. Site selection was carried out such as to obtain a good representation of the diversity of climatic zones and snow cover evolution that can be found in non-mountainous environments. Using three assessment criteria allowed us to more specifically analyze the strengths and weaknesses of MASiN as compared to the other models.

The overall results show that MASiN is substantially more robust than the three reference models, being able to provide comparatively robust snow depth simulation performance even when compared to models that were calibrated at each study site. Aside from performances at two sites, the Nash Sutcliffe coefficients obtained for MASiN showed satisfactory values ranging from 0.63 to 0.89. MASiN also showed the ability to correctly simulate the absence and presence of the snowpack and to rightly evaluate the melt peak occurrence.

At specific sites characterized either by high latitude or significant snow accumulation, MASiN had difficulty achieving the same performance as at other sites, the simulated snow depth being systematically underestimated. The issue of the areal extent validity of a single site parameterization and/or of the use of some equations with geographic-specific applicability is tackled here as climatic conditions for Group 5 are very different from those of other sites.

The parameters set at Dorval provided very good simulation results for the sites in Groups 1, 2 and 3. MASiN exhibited particularly encouraging performances between Sydney and Geraldton in an area covering around 2000 km of longitude and 500 km of latitude. MASiN also proved capable of providing robust simulation results over time even at sites where conditions were highly variable from one winter to another.

Comparing MASiN to two empirical models dedicated to snow depth simulation and a proven mixed degree/day energy-balance snow module from a hydrological model showed the potential of simplified physical snowpack models requiring no or just a few calibrations. However, further evaluations of MASiN's performance should be conducted to complete those presented in the present paper. Among others, MASiN's performance should be compared to that of complex EB models that are recognized as the reference in snow cover modeling and MASiN internal variables such as solar radiation should be compared with physical measurements. Further improvements of MASiN performances and its applicability to hydrological modeling may also require further developments:

- Introduction of different equations for the calculation of snow density and settling.
- Adaptation of MASiN to mountainous environment specificities by adding snow redistribution and coupled slope-orientation effect modules into the model.
- Testing of further MASiN adaptation for hydrological studies by performing direct comparisons of model outputs with SWE or outflow measurements.
- Integration of MASiN into distributed hydrological models in order to check the overall impact on discharge simulation performances.

Overall, this study shows that non-data intensive physically based models such as MASiN can be robust snow models, whose application may be highly beneficial, especially when multi-site calibration is impossible, either because data are lacking or because there are too many uncertainties in terms of calibration validity.

Acknowledgements

This work has been partially funded by the Natural Sciences and Engineering Research Council of Canada. All data used for the evaluation of the model come from the open

access online databases provided by Environment Canada and the Swedish Meteorological and Hydrological Institute.

References

Adam, J.C., Hamlet, A.F., Lettenmaier, D.P., 2009. Implications of global climate change for snowmelt hydrology in the twenty-first century. Hydrol. Process., 23(7): 962-972. DOI:10.1002/hyp.7201

American Meteorological Society, 2012. Bulk Richardson Number. http://glossary.ametsoc.org/wiki/Bulk_richardson_number, Access Date: 2012-08-20

Anderson, E.A., 1976. A point energy and mass balance model of a snow cover. NOAA Technical Report NWS 19, U.S. National Oceanic and Atmospheric Administration, Silver Spring, Maryland.

Armstrong, R.L., Brun, E., 2008. Snow and climate : physical processes, surface energy exchange and modeling. Cambridge University Press, New York, 222 pp.

Arsenault, R., Poulin, A., Côté, P., Brissette, F., 2014. Comparison of stochastic optimization algorithms in hydrological model calibration. Journal of Hydrologic Engineering, 19(7): 1374-1384. DOI:10.1061/(ASCE)HE.1943-5584.0000938

Baraer, M., Madramootoo, C.A., Mehdi, B.B., 2010. Evaluation of winter freeze damage risk to apple trees in global warming projections. Trans. ASABE, 53(5): 1387-1397.

Barnett, T.P., Adam, J.C., Lettenmaier, D.P., 2005. Potential impacts of a warming climate on water availability in snow-dominated regions. Nature, 438(7066): 303-309.

Barry, R., Prévost, M., Stein, J., Plamondon, A.P., 1990. Application of a snow cover energy and mass balance model in a balsam fir forest. Water Resour. Res., 26(5): 1079-1092. DOI:10.1029/WR026i005p01079

Bartelt, P., Lehning, M., 2002. A physical SNOWPACK model for the Swiss avalanche warning Part I: Numerical model. Cold Reg. Sci. Technol., 35(3): 123-145. DOI:10.1016/S0165-232X(02)00074-5

Bavera, D., Bavay, M., Jonas, T., Lehning, M., De Michele, C., 2014. A comparison between two statistical and a physically-based model in snow water equivalent mapping. Adv. Water Res., 63: 167-178. DOI:10.1016/j.advwatres.2013.11.011

Bergström, S., 1976. Development and application of a conceptual runoff model for Scandinavian catchments. SMHI RHO 7, Norrköping, 134 pp.

Bougamont, M., Bamber, J.L., Ridley, J.K., Gladstone, R.M., Greuell, W., Hanna, E., Payne, A.J., Rutt, I., 2007. Impact of model physics on estimating the surface mass balance of the Greenland ice sheet. Geophys. Res. Lett., 34(17), L17501.

Bristow, K.L., Campbell, G.S., 1984. On the relationship between incoming solar radiation and daily maximum and minimum temperature. Agric. For. Meteorol., 31(2): 159-166. DOI:10.1016/0168-1923(84)90017-0

Brubaker, K., Rango, A., Kustas, W., 1996. Incorporating radiation inputs into the snowmelt runoff model. Hydrol. Process., 10(10): 1329-1343.

Brun, E., Martin, E., Simon, V., Gendre, C., Coleou, C., 1989. An energy and mass model of snow cover suitable for operational avalanche forecasting. J. Glaciol., 35(121): 333-342.

Brutsaert, W., 1975. On a derivable formula for long-wave radiation from clear skies. Water Resour. Res., 11(5): 742-744. DOI:DOI:10.1029/WR011i005p00742

Debele, B., Srinivasan, R., Gosain, A.K., 2010. Comparison of Process-Based and Temperature-Index Snowmelt Modeling in SWAT. Water Resour. Manage, 24(6): 1065-1088. DOI:10.1007/s11269-009-9486-2

DeWalle, D.R., Rango, A., 2008. Principles of Snow Hydrology. Cambridge University Press, New York, 410 pp.

Dingman, S.L., 2002. Physical Hydrology. Prentice Hall, New Jersey, 646 pp.

Dorsey, N.E., 1968. Properties of ordinary water-substance in all its phases: water-vapor, water, and all the ices. Monograph series (American Chemical Society)no. 81. Hafner Pub. Co., New York, 673 pp.

Duan, Q., Gupta, V.K., Sorooshian, S., 1993a. A shuffled complex evolution approach for effective and efficient global minimization. J. Optim. Theory Appl., 76(3): 501-521.

Duan, Q., Gupta, V.K., Sorooshian, S., 1993b. A shuffled complex evolution approach for effective and efficient global minimization. Journal of Optimization Theory and Applications, 76(3): 501-521.

Dunkle, R.V., Bevans, J.T., 1956. AN APPROXIMATE ANALYSIS OF THE SOLAR REFLECTANCE AND TRANSMITTANCE OF A SNOW COVER. Journal of Meteorology, 13(2): 212-216. DOI:10.1175/1520-0469(1956)013<0212:aaaots>2.0.co;2

Essery, R., 2015. A factorial snowpack model (FSM 1.0). Geosci. Model Dev., 8(12): 3867-3876. DOI:10.5194/gmd-8-3867-2015

Essery, R., Kontu, A., Lemmetyinen, J., Dumont, M., Ménard, C.B., 2016. A 7-year dataset for driving and evaluating snow models at an Arctic site (Sodankylä, Finland). Geosci. Instrum. Methods Data Sys., 5(1): 219-227. DOI:10.5194/gi-5-219-2016

Essery, R., Morin, S., Lejeune, Y., B Ménard, C., 2013. A comparison of 1701 snow models using observations from an alpine site. Adv. Water Res., 55: 131-148. DOI:http://dx.doi.org/10.1016/j.advwatres.2012.07.013

Farbrot, H., Hanssen-Bauer, I., 2009. A simple station-based empirical model for local snow conditions. The Norwegian Meteorological Institute, Oslo, 19 pp.

Ferguson, R.I., 1999. Snowmelt runoff models. Prog. Phys. Geogr., 23(2): 205-227. DOI:10.1191/030913399672720559

Finger, D., Vis, M., Huss, M., Seibert, J., 2015. The value of multiple data set calibration versus model complexity for improving the performance of hydrological models in mountain catchments. Water Resour. Res., 51(4): 1939-1958. DOI:10.1002/2014WR015712

Förster, K., Meon, G., Marke, T., Strasser, U., 2014. Effect of meteorological forcing and snow model complexity on hydrological simulations in the Sieber catchment (Harz Mountains, Germany). Hydrol. Earth Syst. Sci., 18(11): 4703-4720. DOI:10.5194/hess-18-4703-2014

Franz, K.J., Butcher, P., Ajami, N.K., 2010. Addressing snow model uncertainty for hydrologic prediction. Adv. Water Res., 33(8): 820-832. DOI:10.1016/j.advwatres.2010.05.004

Franz, K.J., Hogue, T.S., Sorooshian, S., 2008. Operational snow modeling: Addressing the challenges of an energy balance model for National Weather Service forecasts. J. Hydrol., 360(1-4): 48-66. DOI:10.1016/j.jhydrol.2008.07.013

Franz, K.J., Karsten, L.R., 2013. Calibration of a distributed snow model using MODIS snow covered area data. J. Hydrol., 494: 160-175. DOI:10.1016/j.jhydrol.2013.04.026

Giddings, J.C., LaChapelle, E., 1961. Diffusion theory applied to radiant energy distribution and albedo of snow. J. Geophys. Res. Atmos., 66(1): 181-189. DOI:DOI:10.1029/JZ066i001p00181

Gray, D.M., Male, D.H., 1981. Handbook of snow : principles, processes, management and use. The Blackburn Press, Caldwell, N.J., 776 pp.

Gubler, H., 1994. Physik von Schnee. Interne Herausgebung, Eidgenössisches Institut für Schnee and Lawinenforschung, Davos (Switzerland).

Hock, R., 2003. Temperature index melt modelling in mountain areas. J. Hydrol., 282(1-4): 104-115. DOI:10.1016/S0022-1694(03)00257-9

Hood, J.L., Hayashi, M., 2015. Characterization of snowmelt flux and groundwater storage in an alpine headwater basin. J. Hydrol., 521(0): 482-497. DOI:http://dx.doi.org/10.1016/j.jhydrol.2014.12.041

Jacobi, H.W., Domine, F., Simpson, W.R., Douglas, T.A., Sturm, M., 2010. Simulation of the specific surface area of snow using a one-dimensional physical snowpack model: Implementation and evaluation for subarctic snow in Alaska. Cryosphere, 4(1): 35-51. DOI:10.5194/tc-4-35-2010

Jordan, R., 1991. A One-dimensional Temperature Model for a Snow Cover, U.S. Army Corps of Engineers, Cold Regions Research and Engineering Laboratory, Special Report 91-16.

Konz, M. et al., 2010. Calibration of a distributed hydrological model for simulations of remote glacierized Himalayan catchments using MODIS snow cover data, Sixth World FRIEND Conference. International Association of Hydrological Sciences Publication 340, pp. 465-473.

Kustas, W.P., Rango, A., Uijlenhoet, R., 1994. A simple energy budget algorithm for the snowmelt runoff model. Water Resour. Res., 30(5): 1515-1527. DOI:10.1029/94WR00152

Langlois, A. et al., 2009. Simulation of snow water equivalent (SWE) using thermodynamic snow models in Québec, Canada. J. Hydrometeorol., 10(6): 1447-1463. DOI:10.1175/2009JHM1154.1

Lee, R., 1963. Evaluation of solar beam irradiation as a climatic parameter of mountain watersheds. Hydrology Papers of the Colorado State University(2).

Linacre, E., 1992. Climate Data and Resources: A Reference and Guide. Routledge, London, 366 pp.

Liston, G.E., Elder, K., 2006. A distributed snow-evolution modeling system (snowmodel). J. Hydrometeorol., 7(6): 1259-1276. DOI:10.1175/JHM548.1

Ludwig, R. et al., 2009. The role of hydrological model complexity and uncertainty in climate change impact assessment. Adv. Geosci., 21: 63-71. DOI:10.5194/adgeo-21-63-2009

Lundberg, A. et al., 2016. Snow and frost: Implications for spatiotemporal infiltration patterns - a review. Hydrol. Process., 30(8): 1230-1250. DOI:10.1002/hyp.10703

Machguth, H., Paul, F., Hoelzle, M., Haeberli, W., 2006. Distributed glacier mass-balance modelling as an important component of modern multi-level glacier monitoring. Ann. Glaciol., 43: 335-343. DOI:10.3189/172756406781812285

Magnusson, J., Gustafsson, D., Hüsler, F., Jonas, T., 2014. Assimilation of point SWE data into a distributed snow cover model comparing two contrasting methods. Water Resour. Res., 50(10): 7816-7835. DOI:10.1002/2014WR015302

Martinec, J., Rango, A., 1986. Parameter values for snowmelt runoff modelling. J. Hydrol., 84(3-4): 197-219. DOI:10.1016/0022-1694(86)90123-X

Mauser, W., Bach, H., 2009. PROMET - Large scale distributed hydrological modelling to study the impact of climate change on the water flows of mountain watersheds. J. Hydrol., 376(3-4): 362-377. DOI:10.1016/j.jhydrol.2009.07.046

Meeks, J., Moeck, C., Brunner, P., Hunkeler, D., 2017. Infiltration under snow cover: Modeling approaches and predictive uncertainty. J. Hydrol., 546: 16-27. DOI:10.1016/j.jhydrol.2016.12.042

Mendoza, P.A., Rajagopalan, B., Clark, M.P., Cortés, G., McPhee, J., 2014. A robust multimodel framework for ensemble seasonal hydroclimatic forecasts. Water Resour. Res., 50(7): 6030-6052. DOI:10.1002/2014WR015426

Minder, J.R., 2010. The Sensitivity of Mountain Snowpack Accumulation to Climate Warming. J. Clim., 23(10): 2634-2650. DOI:10.1175/2009JCLI3263.1

Morin, S., 2014. Observation and numerical modeling of snow on the ground: use of existing tools and contribution to ongoing developments, Université Joseph Fourier, Grenoble, 95 pp.

Mosier, T.M., Hill, D.F., Sharp, K.V., 2016. How much cryosphere model complexity is just right? Exploration using the conceptual cryosphere hydrology framework. Cryosphere, 10(5): 2147-2171. DOI:10.5194/tc-10-2147-2016

Nash, J.E., Sutcliffe, J.V., 1970. River flow forecasting through conceptual models part I - A discussion of principles. J. Hydrol., 10(3): 282-290. DOI:10.1016/0022-1694(70)90255-6

Navarre, J.P., 1975. Modèle unidimensionnel d'évolution de la neige déposée. Modèle perce-neige. Météorologie, 4(3): 17.

Ohara, N., Kavvas, M.L., 2006. Field observations and numerical model experiments for the snowmelt process at a field site. Adv. Water Res., 29(2): 194-211. DOI:10.1016/j.advwatres.2005.03.016

Oke, T.R., 2002. Boundary Layer Climates. Routledge, 464 pp.

Pellicciotti, F. et al., 2005. An enhanced temperature-index glacier melt model including the shortwave radiation balance: development and testing for Haut Glacier d'Arolla, Switzerland. J. Glaciol., 51(175): 573-587.

Pohl, S., Marsh, P., Bonsal, B.R., 2006. Modeling the Impact of Climate Change on Runoff and Annual Water Balance of an Arctic Headwater Basin. Arctic, 60(2): 173 - 186.

Raleigh, M.S., Livneh, B., Lapo, K., Lundquist, J.D., 2016. How does availability of meteorological forcing data impact physically based snowpack simulations? J. Hydrometeorol., 17(1): 99-120. DOI:10.1175/JHM-D-14-0235.1

Rutter, N. et al., 2009. Evaluation of forest snow processes models (SnowMIP2). J. Geophys. Res. Atmos., 114(6). DOI:10.1029/2008JD011063

Saelthun, N.R. et al., 1998. Climate change impacts on runoff and hydropower in the Nordic countries. Final report from the project "Climate Change and Energy Production". Tema Nord 1998, Nordic Council of Ministers, Copenhagen.

Scott, D., McBoyle, G., Mills, B., 2003. Climate change and the skiing industry in southern Ontario (Canada): Exploring the importance of snowmaking as a technical adaptation. Clim. Res., 23(2): 171-181.

Sergent, C., Chevrand, P., Lafeuille, J., Marbouty, D., 1987. Caracterisation optique de differents types de neige. Extinction de la lumière dans la neige. J. Phys. Colloques, 48(C1): 361-367.

Shamir, E., Georgakakos, K.P., 2006. Distributed snow accumulation and ablation modeling in the American River basin. Adv. Water Res., 29(4): 558-570. DOI:10.1016/j.advwatres.2005.06.010

Singh, P.R., Gan, T.Y., Gobena, A.K., 2009. Evaluating a hierarchy of snowmelt models at a watershed in the Canadian Prairies. J. Geophys. Res. Atmos., 114(4). DOI:10.1029/2008JD010597

Stone, R.S., Dutton, E.G., Harris, J.M., Longenecker, D., 2002. Earlier spring snowmelt in northern Alaska as an indicator of climate change. J. Geophys. Res. Atmos., 107(9-10): 10-1.

Strasser, U., Marke, T., 2010. ESCIMO.spread - A spreadsheet-based point snow surface energy balance model to calculate hourly snow water equivalent and melt rates for historical and changing climate conditions. Geosci. Model Dev., 3(2): 643-652. DOI:10.5194/gmd-3-643-2010

Sturm, M., 2015. White water: Fifty years of snow research in WRR and the outlook for the future. Water Resour. Res., 51(7): 4948-4965. DOI:10.1002/2015WR017242

Sturm, M. et al., 2010. Estimating snow water equivalent using snow depth data and climate classes. J. Hydrometeorol., 11(6): 1380-1394. DOI:10.1175/2010JHM1202.1

Thompson, L.G. et al., 2000. A High-Resolution Millennial Record of the South Asian Monsoon from Himalayan Ice Cores. Science, 289(5486): 1916-1919. DOI:10.1126/science.289.5486.1916

Tobin, C. et al., 2013. Improving the degree-day method for sub-daily melt simulations with physically-based diurnal variations. Adv. Water Res., 55: 149-164. DOI:10.1016/j.advwatres.2012.08.008

Troin, M., Poulin, A., Baraer, M., Brissette, F., 2016. Comparing snow models under current and future climates: Uncertainties and implications for hydrological impact studies. J. Hydrol., 540: 588-602. DOI:10.1016/j.jhydrol.2016.06.055

Turcotte, R., Fortin, L.G., Fortin, V., Fortin, J.P., Villeneuve, J.P., 2007. Operational analysis of the spatial distribution and the temporal evolution of the snowpack water equivalent in southern Québec, Canada. Nord. Hydrol., 38(3): 211-234.

U.S. Army Corps of Engineers, 1956. Snow hydrology : Summary report of the snow investigations. Technical report. U.S. Army Corps of Engineers, North Pacific Division, Portland, Oregon.

Valéry, A., 2010. Modélisation précipitations – débit sous influence nivale. Elaboration d’un module neige et évaluation sur 380 bassins versants. Ph. D. Thesis, AgroParisTech, Paris, 405 pp.

Warscher, M. et al., 2013. Performance of complex snow cover descriptions in a distributed hydrological model system: A case study for the high Alpine terrain of the Berchtesgaden Alps. Water Resour. Res., 49(5): 2619-2637. DOI:10.1002/wrcr.20219

Watson, B.M., Putz, G., 2014. Comparison of Temperature-Index Snowmelt Models for Use within an Operational Water Quality Model. J Environ Qual, 43(1): 199-207. DOI:10.2134/jeq2011.0369

Williams, K.S., Tarboton, D.G., 1999. The ABC's of snowmelt: A topographically factorized energy component snowmelt model. Hydrol. Process., 13(12-13): 1905-1920.

Yen, Y.C., 1981. Review of thermal properties of snow, ice, and sea ice. Technical report. U.S. Army Corps of Engineers, Cold Regions Research and Engineering Laboratory, Hanover, New Hampshire.